Hyperfine Interact (2016) 237:60
DOI 10.1007/s10751-016-1233-5

Mössbauer and electrical conduction investigations of LiFe(BaTi)(PO_4) NASICON nano composite

M. Y. Hassaan[1] · Zhu Kaixin[2] · Junhu Wang[2] · M. G. Moustafa[1]

Abstract NASICON glass sample with a composition of $Li_{1.3}Fe_{0.3}(BaTi)_{1.7}(PO_4)_3$ was prepared using the conventional melt-quenching technique at 1300 °C for one hour after two stages of calcination process at 300 °C and 600 °C respectively. DTA was used to determine (T_g) and (T_c) of the as-quenched glass sample. XRD was used to confirm the glassy state of the prepared sample. The as-quenched glass sample was heat treated near its onset crystallization temperature for different times 1, 2, 3, 4, and 5 hours. The gradual precipitation of the crystalline nano-particles with NASICON type structure was also confirmed using XRD. The as-prepared sample and the five heat treated (HT) samples were investigated using Mössbauer spectroscopy, DC and AC conductivities and dielectric permittivity. FTIR, density, and TEM measurements were also performed. After HT, XRD and FTIR measurements conformed the formation of NASICON phase. The results of the dielectric permittivity showed no maximum peak in the studied temperature and frequency ranges, which indicates the absence of ferroelectric behavior of the HT glass sample. Mössbauer data showed that the iron in the glass and its HT samples include two ionic states, Fe^{3+} (O_h) and Fe^{2+} (O_h) ions. It is observed that the DC conductivity of the HT glass for 5 h was almost two orders of magnitude higher than that of the parent glass.

Keywords NASICON-type · $Li_3Ti_2(PO_4)_3$ · Ionic conductivity · Heat treatment · Dielectric studies · AC conductivity

This article is part of the Topical Collection on *Proceedings of the International Conference on the Applications of the Mössbauer Effect (ICAME 2015), Hamburg, Germany, 13–18 September 2015*

✉ M. G. Moustafa
myhassaan@yahoo.com

[1] Physics Department, Faculty of Science, Al-Azhar University, Nasr City 11884, Cairo, Egypt

[2] Laboratory of Catalysts and New Materials for Aerospace, Dalian Institute of Chemical Physics Chinese, Academy of Sciences, 457 Zhongshan Road, Dalian 116023, China

Published online: 24 February 2016

1 Introduction

NASICON ceramics have attracted increasing attention of many scientists with the last two decades according to their enhanced ionic conductivity which is useful in different fields of applications such as ion selective electrodes, solid batteries etc. [1–5]. At present, Li^+ ion rechargeable batteries represent the most power sources for different modern portable electronic devices [6–8]. The high energy efficiency of Li-ion batteries may also allow their use in various electronic grid applications [5]. Glass from lithium and a transition metal ions such as vanadium with other glass forming oxide like P_2O_5 or SiO_2 exhibit high mixed electronic-ionic conduction due to mobility of Li^+ ions and the electronic conduction produced from electron hopping from V^{4+} to V^{5+} according to Mott [9].

The glass forming ability of the Li_2O–TiO_2–P_2O_5 system glasses was investigated by Kishioka. He has identified the restricted glass-forming regions of this system [10]. Glass-ceramics belonging to the Li_2O–TiO_2–P_2O_5 system exhibit superior properties such as ionic conductivity [11] and ion-exchange capacity [12] due to the formation of an alkali or alkaline-earth titanium phosphate phase which is called NASICON [12–15]. Ionic – Electronic conducting characteristics of $LiFePO_4$ cathode materials were studied [16].

The formation of nanocrystals inside glass matrix is due to heat treatment of glass sample near its crystallization temperature for a short time (1-5 h). These nanocrystals in glass structure (which may call nanocomposite) improve the physical properties specially the electrical conductivity. Lithium phosphate glasses could be used as fast ionic conductor. When transition metal ions present in such glass, electronic conduction may be observed [17, 18].

The aim of the present work is to explore the HT glass with high ionic conductivity in NASICON framework and detecting Fe^{2+} and Fe^{3+} ions using Mössbauer spectrometer which may cause electronic conduction according to small polaron hopping. Also, the dielectric property of our samples should be examined to recognize the presence of ferroelectric behavior for our samples.

2 Experimental

The glass sample of composition $Li_{1.3}Fe_{0.3}(BaTi)_{1.7}(PO_4)_3$ was prepared by conventional melt quenching technique from analytical reagent grade chemicals Li_2CO_3, $BaCO_3$, TiO_2, Fe_2O_3 and $NH_4H_2PO_4$ according to our previous work [1, 2].

On the other hand, Glass–ceramics were prepared by heating the glass plates close to its onset crystallization temperature (i.e. at 600 °C) for different times 1, 2, 3, 4, and 5 hours on the basis of the observed DTA results, using Shimadzu (DTA) instrument. The bulk densities were measured at room temperature using Archimedes method with carbon tetrachloride as the immersing liquid (1.593 $g.cm^{-3}$). X-ray diffraction (XRD) measurements of the glass sample and their corresponding glass–ceramics were conducted using [Rigaku RINT 2100] with [Cukα = 0.1541 nm] radiation. The maximum current and voltage were 300 mA and 50 kV. FT-IR spectra were measured for all samples in range (400 – 4000 cm^{-1}) using computerized FT-IR spectrophotometer JASCO [FT-IR-300E] and using KBr as a reference material.

The TEM (model: JEOL Jem-1010) is used to investigate the nanostructure of HT glass sample and to demonstrate the amorphous nature of glass sample. The DC electrical conductivity, on the other hand, for glass sample and their corresponding glass–ceramics were measured by means of the two-probe method, which is appropriate for high resistance

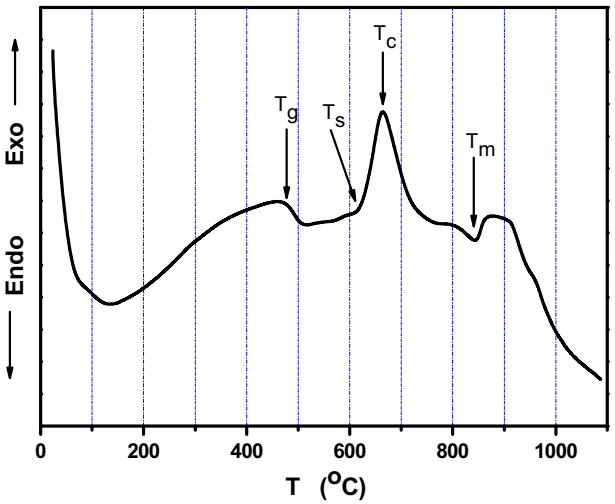

Fig. 1 DTA Curve of $Li_{1.3}\ Fe_{0.3}(BaTi)_{1.7}(PO_4)_3$ glass

Table 1 Glass transition temperature (T_g), onset crystallization temperature (T_s), crystallization peak temperature (T_c), melting temperature (T_m), and thermal stability parameters (ΔT, S, T_g/T_m) for the glass sample

Sample	T_g (°C) ±2	T_s (°C) ±2	T_c(°C) ±2	T_m (°C) ±2	ΔT ±2	S ±2	T_g/T_m
Glass	470	618	664	843	148	18.99	0.56

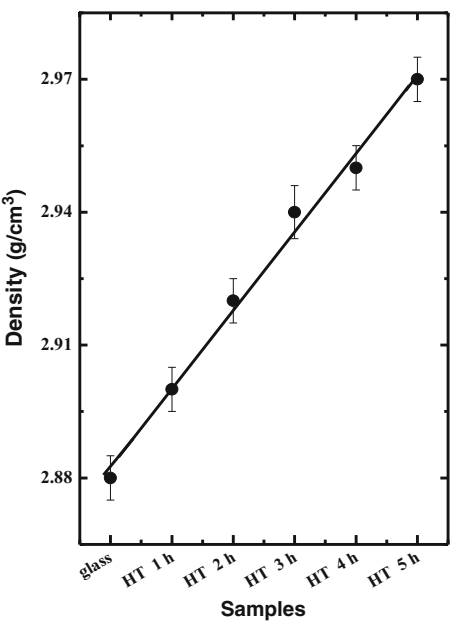

Fig. 2 Density of as prepared glass and HT glass samples

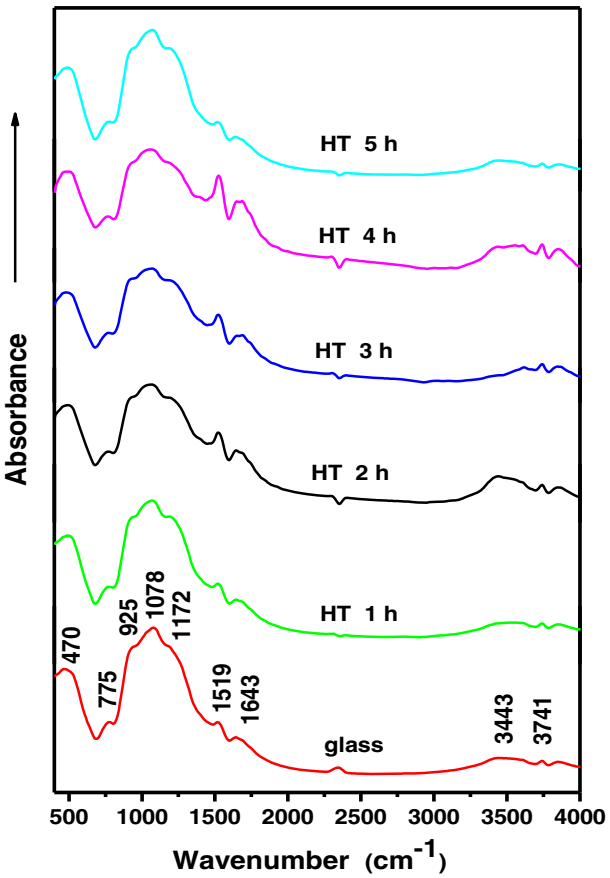

Fig. 3 FTIR absorption spectra of $Li_{1.3}$ $Fe_{0.3}(BaTi)_{1.7}(PO_4)_3$ glass and HT glass samples

materials. Silver painted electrodes were pasted on the polished surface of the samples and then situated between two polished and cleaned copper electrodes. KEITHLEY 485 Autoranging Pico Ameter was used to collect the DC data over the temperature range (300-600 K). The sample temperature was measured by a chromal–alumal type K thermocouple which is placed as close as possible to the sample. The AC conductivity and dielectric constant of the glass and HT samples were measured using LRC Tester (HIOKI, 50-3532). Room temperature ^{57}Fe Mössbauer spectra were recorded by using a Topologic 500A spectrometer and a proportional counter. ^{57}Co (Rh) moving with a constant acceleration mode was used as the γ-ray radioactive source.

3 Results and discussion

3.1 DTA

DTA is a versatile technique to identify the characteristic temperatures for the studied samples. The DTA curve shown in Fig. 1 was obtained for the as prepared glass (powder)

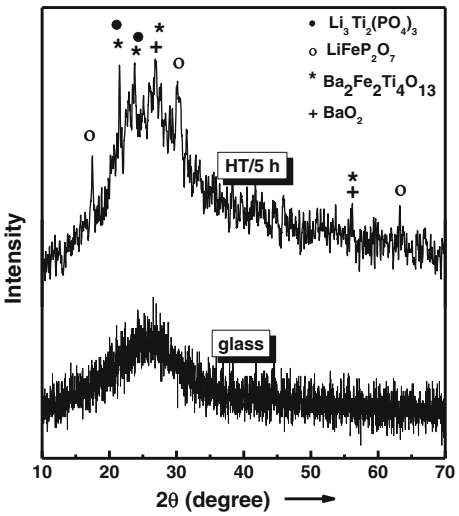

Fig. 4 XRD of $Li_{1.3}Fe_{0.3}(BaTi)_{1.7}(PO_4)_3$ glass and HT/5 h samples

corresponding to the composition $Li_{1.3}Fe_{0.3}(BaTi)_{1.7}(PO_4)_3$. The DTA trace alternatively was obtained for the sample which confirmed the glassy nature. The figure exhibits endothermic minimum which represents the glass transition temperature (Tg) at around 470 °C, the onset crystallization temperature (T_s) at around at 618 °C and successive exothermic peak corresponding to crystallization temperature (T_c) at around 664 °C, followed by endothermic effect due to the re-melting of the glass (T_m) at around 843 °C. The significant difference that exists between the glass transition, T_g and the onset of the crystallization temperature T_s accounts the thermal stability of the glass sample. The thermal stability (ΔT) parameter is usually employed to estimate the glass durability [1, 19] which is defined by

$$\Delta T = T_s - T_g \tag{1}$$

While according to Saad and Poulain [1, 20] the thermal stability parameter (S) which reflects the resistance for devitrification of glass and it is defined by

$$S = (T_c - T_s)(T_c - T_g)/T_g \tag{2}$$

In the above equation ($T_c - T_s$) is the rate of devitrification transformation of glassy phase. The values of ΔT and S, calculated from (1) and (2) respectively, are presented in Table 1. This reveals that the glass sample has high thermal stability and good glass forming ability.

On the other hand, the factor T_g/T_m (ratio of the glass transition to the melting temperatures) exhibits a good measure of the glass stability, which has an ideal value of about 0.66 for stable glass. The T_g/T_m value is 0.56 for the glass sample in the present investigation, indicating its moderate thermal stability [21, 22].

3.2 Density

The density of the material is an important property to understand the structure and many other properties which are useful in many industries. Figure 2 shows density of as prepared glass and HT glass samples. It is noted that, the density of HT glass is greater than that of the parent glass. The increase in density of HT glass may be due to the rearrangement

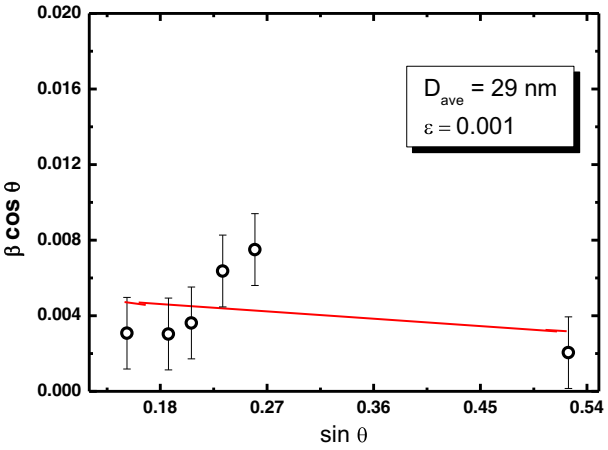

Fig. 5 W-H plot for HT/5 h sample

of some glass forming ions causing structural changes in glass-ceramic, which are more closely packed than in glass network [1].

3.3 Fourier-transform infrared spectroscopy

In order to determine the main features concerning the local structure of the samples under study, a series of FTIR absorption measurements were carried out. FTIR absorption spectra of $Li_{1.3}Fe_{0.3}(BaTi)_{1.7}(PO_4)_3$ system are shown in Fig. 3. FTIR spectra of all samples obviously show six main bands at ∼470, 1078, 1519, 1643, 3443 and 3741 cm^{-1} in addition to three shoulders at ∼775, 925 and 1172 cm^{-1}. The band at ∼470 cm^{-1} is assigned to asymmetric bending vibration modes of O–P–O units [23, 24]. After HT for different times this band shifted to higher wavenumbers. The shoulder at 775 cm^{-1} is attributed to symmetric stretching vibrations of P–O–P bridging bonds in pyrophosphate $(P_2O_7)^{4-}$ units [25].

The bands at ∼925 and 1078 cm^{-1} indicate the presence of the $(PO_4)^{3-}$ ionic group vibration [24, 26]. Generally the vibrational modes of NASICON phases can be assigned to PO_4 tetrahedral (internal and external modes) and to lattice modes of metal octahedral. Accordingly, the bands corresponding to PO_4 unit are intense than metal octahedral bands [1]. Thus, the presence of the $(PO_4)^{3-}$ ionic group indicates the formation of NASICON phase. The observed band at ∼1172 cm^{-1} may be identified as to the $(P–O)^{(-)}$ ionic vibration [24, 27, 28]. The observed bands in the region 1519–1643 cm^{-1} is due to the deformation vibration modes of the H_2O [24, 29]. Besides, the bands in the region 3443–3741 cm^{-1} is due to the stretching vibration modes of the OH [29].

3.4 X-ray diffraction (XRD)

Figure 4 represents the XRD patterns of the glass and HT/5 h glass samples. The absence of the Bragg peaks confirms the amorphous inherence of the fabricated glass sample. In case of HT/5 h some peaks are observed and they are identified to be $Li_3Ti_2(PO_4)_3$ (JCPDS card 40–0095) with a structure close to rhombohedra (NASICON phase), $LiFe(P_2O_7)$ (JCPDS card 80–1371) with a structure close to monoclinic, $Ba_2Fe_2Ti_4O_{13}$ (JCPDS card 87–1480)

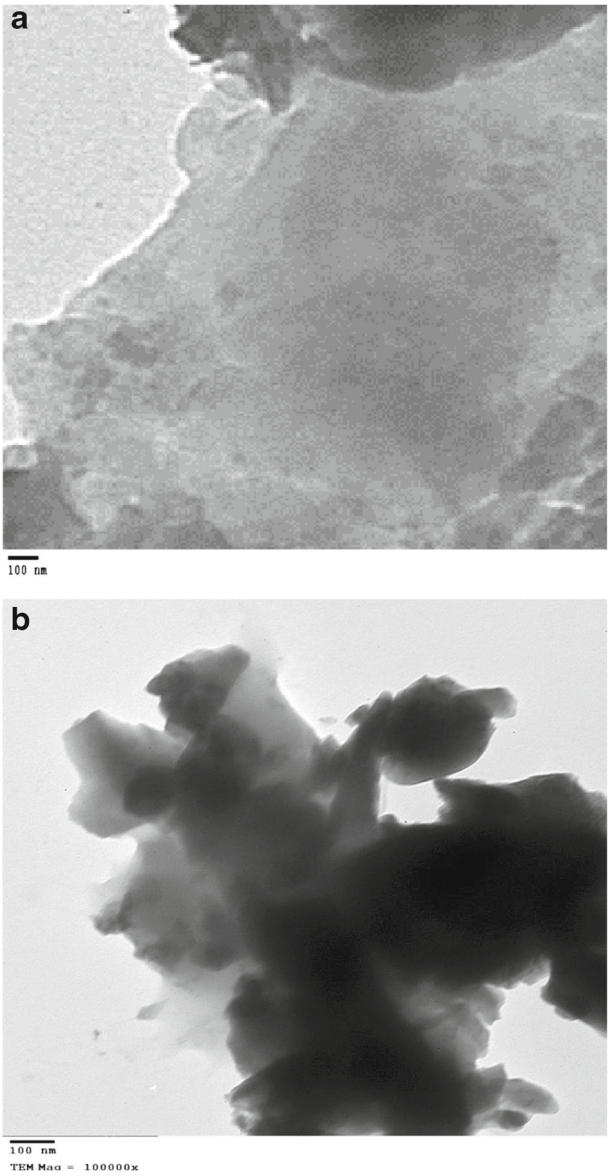

Fig. 6 Typical TEM graphs for (**a**) glass sample (**b**) HT/5 h sample

with a structure close to monoclinic and BaO_2 (JCPDS card 73–1739) with a structure close to tetragonal.

In this regards, it was expected that Ti ions replaced by Fe ions within NASICON structure due to their comparable ionic radii. This substitution could provide more lithium mobile ions inside the framework of conduction channels. Particular attention should also been paid to likely effects of iron ions as nucleating agent for precipitation of NASICON phase. The

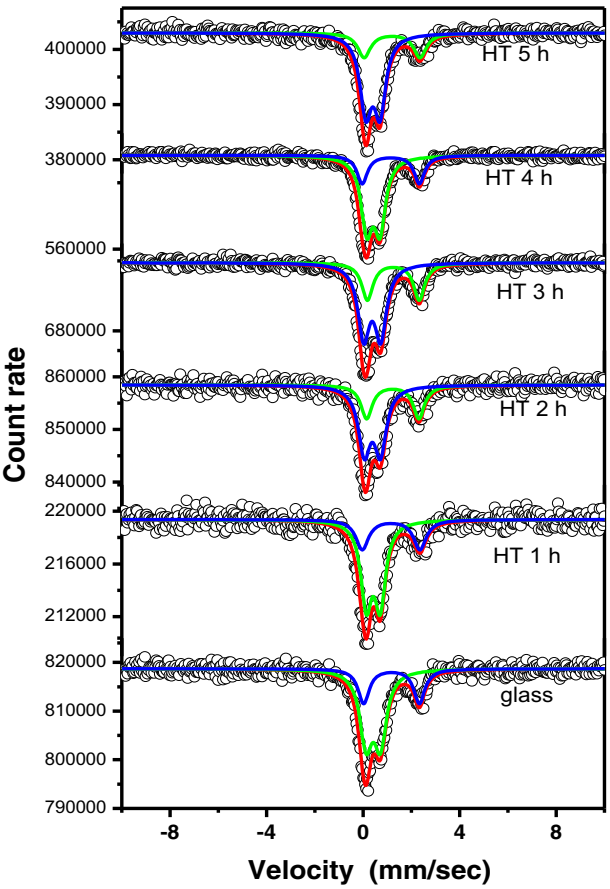

Fig. 7 Mössbauer spectra at room temperature of $Li_{1.3}Fe_{0.3}(BaTi)_{1.7}(PO_4)_3$ glass and HT samples

Table 2 Mössbauer parameters of the obtained Mössbauer spectra exhibited in Fig. 7

Samples	Fe^{3+} (Oh)				Fe^{2+} (Oh)			
	IS (mms^{-1})	QS (mms^{-1})	LW (mms^{-1})	A (%)	IS (mms^{-1})	QS (mms^{-1})	LW (mms^{-1})	A (%)
Glass	0.42	0.59	0.40	69.4	1.18	2.31	0.36	30.6
HT 1 h	0.42	0.58	0.40	70.0	1.16	2.39	0.35	30.0
HT 2 h	0.40	0.56	0.40	67.0	1.23	2.16	0.37	33.0
HT 3 h	0.41	0.56	0.39	66.7	1.25	2.15	0.36	33.3
HT 4 h	0.42	0.55	0.38	72.6	1.15	2.37	0.35	27.4
HT 5 h	0.40	0.59	0.38	73.5	1.20	2.31	0.36	26.5

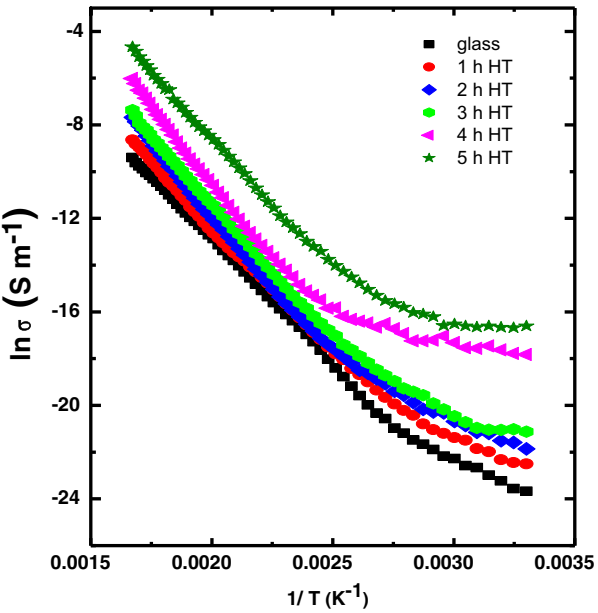

Fig. 8 The temperature dependence of DC conductivity for glass and HT samples

average crystallite size is calculated from Williamson–Hall (W-H) plot between $\beta \cos\theta$ and $\sin\theta$ as given in Fig. 5, using XRD data. The Williamson–Hall [1, 30] equation is:

$$\beta \cos\theta = \frac{c\lambda}{D_{ave}} + 4\varepsilon \sin\theta \tag{3}$$

where β is the full width at half maximum (FWHM), θ is the Bragg angle, C is the correction factor ($c \approx 1$), D_{ave} is the average crystallite size, λ is the wavelength of X-ray, ε is the lattice strain. The average crystallite size was found equal 29 nm and the lattice strain is equal 0.001.

3.5 TEM

TEM is used to understand the changes of the structure of the present system. Typical TEM along with the selective area for glass and HT/5h samples is shown in Fig. 6. In case of glass sample Fig. 6a exhibits area without the presence of microstructure which is characteristic for the amorphous phase. In case of HT/5h Fig. 6b shows nanocrystallites of different sizes (30–40 nm) embedded in the glass matrix. The crystallite size is agree with or close to XRD results.

3.6 Mössbauer spectroscopy

Figure 7 showed Mössbauer spectra at room temperature of all samples. The hyperfine parameters are reported in Table 2. From The hyperfine parameters we can observe that our glass and its HT samples contain two ionic states of iron, Fe^{3+} octahedral (O_h) ions and

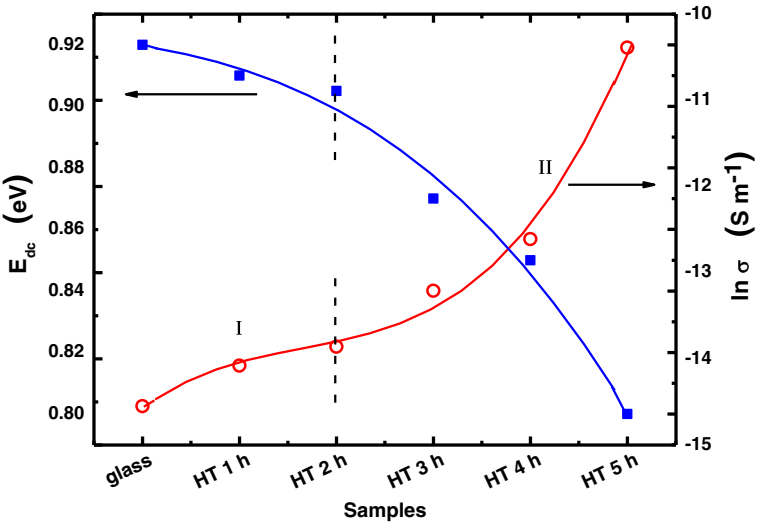

Fig. 9 Variation of DC conductivity at 463 K and the high temperature activation energy for glass and HT samples

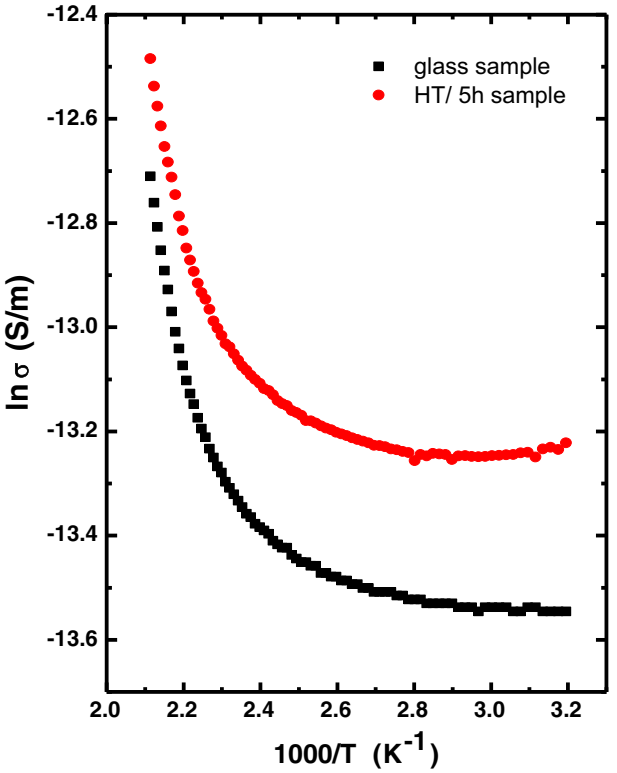

Fig. 10 The temperature dependence of AC conductivity at 1000 Hz for glass and HT/5 h samples

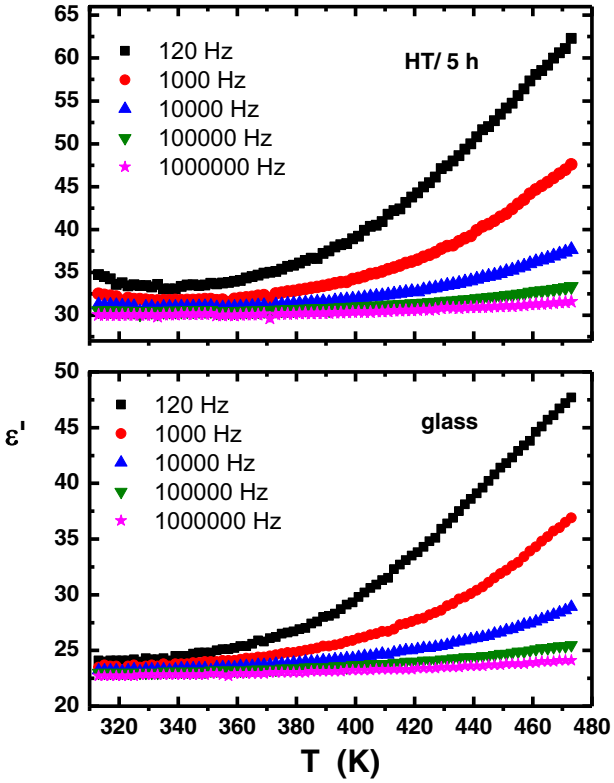

Fig. 11 The temperature dependence of real part of dielectric constant (ε') at different frequencies for glass and HT/5 h samples

Fe^{2+} (O_h) ions. These two iron cations are found in the glass network and further more in two of the precipitated phases after HT according to XRD results.

3.7 DC electrical conductivity

Figure 8 shows the temperature dependence of DC conductivity for as prepared glass and its HT samples. The dependence of ln σ on 1/T is characterized by two temperature regions. The first is the lower temperature region (up to 377 K), where the conductivity increases slightly with temperature and is attributed to electronic conduction mechanism due to the small polaron hopping from the lower valance state ion to the higher valance state of iron (Mott). The second region is the higher temperature region, where the conductivity increases with higher rate as the temperature increases and is due to ionic conduction mechanism through the Li^+ ions.

The activation energy, E_{dc}, in higher temperature region for all samples was calculated from the slope of the Arrhenius plots. The activation energy, E_{dc}, and DC conductivity, at 463K are plotted as a function of the studied samples in Fig. 9. From this figure it is clear that the magnitude of the conductivity at fixed temperature (463K) increases gradually with increasing HT times. Also, it is clear that the rate of increasing of conductivity is not constant. In region (I) the conductivity increases slightly (almost constant) but in region (II) the

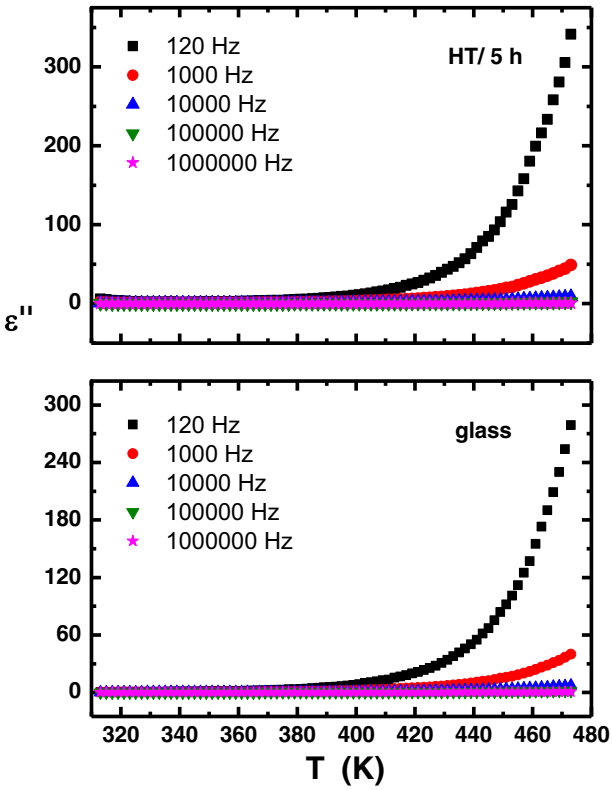

Fig. 12 The temperature dependence of imaginary part of dielectric constant (ε'') at different frequencies for glass and HT/5 h samples

conductivity increases with higher rate than the first. This is may be due to the increase in mobility of charge carriers which is small in region (I) and is higher in region (II) according to the increase in HT times. It is observed that the conductivity of the HT/5 h sample was almost two orders of magnitude higher than that of the parent glass. The enhancement of the conductivity may be attributed to the formation of the conducting crystalline phase with NASICON-type structure after HT process, together with the percolation effect of the remaining matrix glass. As known, glass ceramics generally consist of small amounts of residual glass and crystalline grains, which are embedded in the glass matrix. Consequently, when the NASICON-type structure formed in the grains, the polycrystalline grains provided suitable channels for the migration of Li^+ ions which causing enhancement of its mobility. Furthermore, due to the orientated effect of the NASICON-type grains, the first few atomic layers of glass matrix surrounding the grains perhaps have a near-NASICON structure. Accordingly, the amorphous phase between any two crystalline grains behaved almost like NASICON phase. As a result, percolation paths were created in the remaining amorphous phase [1, 31, 32]. Therefore, the energy barrier for mobile ions in the case of glass ceramics was much smaller than that of the parent glass and an enhancement in the ionic conductivity was observed. It is worthy result for different applications that we found the ionic conductivity of our samples have value at temperature close to room temperature.

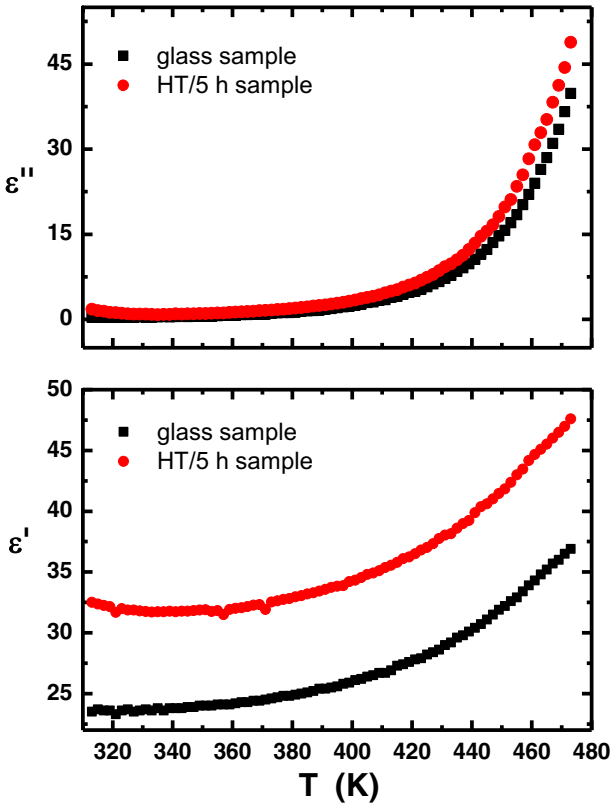

Fig. 13 The temperature dependence of real (ε') and imaginary (ε'') part of dielectric constant at 1000 Hz for glass and HT/5 h samples

Therefore, further detailed study on the conductivity of these samples should be focused on lower temperatures region in our next work.

3.8 AC conductivity

Figure 10 showed the temperature dependence of AC conductivity at 1000 Hz for glass and HT/5 h samples. It is observed that, AC conductivity exhibits the same behavior of the DC results where a very slow increasing rate at low temperatures and then a fast rate at higher temperatures appeared. This is proving that the conduction mechanism is the same in both lower and higher temperatures regions. Also, it is noted that, AC conductivity of HT/5 h sample is much higher than that of as prepared glass sample.

3.9 Dielectric studies

Figure 11 shows the temperature dependence of real part of dielectric constant (ε') at different frequencies for glass and HT/5 h samples. It is observed that, the real part of dielectric constant for glass and HT/5 h samples increases with increasing temperature. This behavior is typical to the polar dielectrics in which the orientation of dipoles is facilitated with rising temperature and thereby the dielectric constant is increased. Also, it is observed that,

the real part of dielectric constant for glass and HT/5 h samples decreases with increasing frequency. This is due to decrease in dipole polarization [33].

On the other hand, the temperature dependence of imaginary part of dielectric constant (ε'') at different frequencies for glass and HT/5 h samples is shown in Fig. 12. It is clear that, the imaginary part exhibits the same behavior of real part of dielectric constant.

Figure 13, showed that the dielectric constant (real and imaginary) of HT/5 h sample is higher than that in glass sample. At the crystallization temperature the ions indulge in rapid movement to transform from a random or glassy to ordered crystalline state and hence the higher dielectric constant via higher polarization. The results of the dielectric permittivity showed no maximum peak in the temperature and frequency range studied, which indicates a non-ferroelectric behavior of the HT glass sample [34].

4 Conclusion

Glass sample of composition $Li_{1.3}Fe_{0.3}(BaTi)_{1.7}(PO_4)_3$ was prepared by a conventional melt-quenching method. Glass–ceramic nanocomposites were obtained by heat treatment of glass according to DTA results for different times. The DTA curve confirmed the amorphous nature of glass sample. Also, DTA results reveal that the glass sample has high thermal stability and good glass forming ability. Therefore, this sample could be used in a lot of modern applications. XRD and FTIR confirmed the forming NASICON phase. TEM and XRD demonstrate the precipitated phase in nano-scale. It is observed that the conductivity of the HT/5 h sample is much higher than that of the parent glass. The results of the dielectric permittivity showed no maximum peak in the studied temperature and frequency ranges, which indicates the absence of ferroelectric behavior of the HT glass sample. Mössbauer data showed that the iron in the glass and its HT samples include two ionic states, Fe^{3+} (O_h) and Fe^{2+} (O_h) ions.

Acknowledgments The authors would like to thank Prof. M. M. El- Desoky and Prof. I. Kashif for their efforts.

References

1. Hassaan, M.Y., Salem, S.M., Moustafa, M.G.: J. Non-Cryst. Solids **391**, 6–11 (2014)
2. Hassaan, M.Y., Salem, S.M., Moustafa, M.G., Kubuki, S., Matsuda, K., Nishida, T.: Hyperfine Interact. **226**, 131–140 (2014)
3. Hassaan, M.Y., Moustafa, M.G., Salem, S.M., Amer, T.Z., Mostafa, A.G.: Presented in Mediterranean Conference on the Applications of the Mössbauer Effect (MECAME 2015), held in Zadar, Croatia (2015)
4. Hassaan, M.Y., El-Desoky, M.M., Moustafa, M.G., Iida, Y., Kubuki, S., Nishida, T.: Presented in Mediterranean Conference on the Applications of the Mössbauer Effect (MECAME 2015), held in Zadar, Croatia (2015)
5. Nitta, N., Wu, F., Lee, J.T., Yushin, G.: Mater. Today **18**, 252 (2015)
6. Wakihara, M.: Mater. Sci. Eng., R **33**, 109 (2001)
7. Wang, G.X., Bewlay, B., Yao, J., Chen, Y., Guo, Z.P., Liu, H.K., Dou, S.X.: J. Power Sources **119**, 189 (2003)
8. Sarre, G., Blanchard, P., Broussely, M.: J. Power Sources **127**, 65 (2004)
9. Mott, M.F.: Adv. Phys. **6**, 16–49 (1967)
10. Kishioka, A.: Bull. Chem. Soc. Jpn. **51**(9), 2559–2561 (1978)
11. Hosono, H., Abe, Y.: J. Am. Ceram. Soc. **75**, 2862–2864 (1992)
12. Hosono, H., Tsuchitani, F., Imai, K., Abe, Y.: J. Mater. Res. **9**(3), 755–761 (1994)

13. Xu, X., Wen, Z., Yang, X., Zhang, J., Gu, Z.: Solid State Ionics **177**, 2611–2615 (2006)
14. Yamamoto, K., Abe, Y.: J. Am. Ceram. Soc. **81**(8), 2201–2204 (1998)
15. Yamamoto, K., Abe, Y.: Mater. Res. Bull. **35**(2), 211–216 (2000)
16. Wang, C., Hong, J.: Electrochem. Solid-State Lett. **10**(3), A65–A69 (2007)
17. Nishida, T., Fukuda, K., Ikeda, A.: Croat. Chem. Acta **77**(1-2), 259–262 (2004)
18. Nishida, T., Yoshida, Y., Takahashi, Y., Okada, S., Yamaki, J.: J. Radioanal. Nucl. Chem. **275**(2), 417–422 (2008)
19. Mahadevan, S., Giridhar, A., Singh, A.K.: J. Non-Cryst. Solids **88**, 11 (1986)
20. Saad, M., Poulain, M.: Mater. Sci. Forum **19&20**, 11 (1987)
21. Sakka, S., Mackenzie, J.D.: J. Non-Cryst. Solids **6**, 145–162 (1991)
22. Bahgat, A.A., Moustafa, M.G., Shaisha, E.E.: J. Mater. Sci. Technol. **29**(12), 1166–1176 (2013)
23. Nakaumoto, K.: Infrared and Raman Spectra of Inorganic and Coordination Com-Pounds: Part A, Theory and Applications in Inorganic Chemistry. Wiley, New York (1997)
24. Dayanand, C., Bhikshamaiah, G., Jayatyagareju, V., Salagram, M., Krishnamurthy, A.S.R.: J. Mater. Sci. **31**, 1945 (1996)
25. Nyquist, R.A., Putzig, C.L., Leugers, M.A.: Infrared and Raman Spectral Atlas of Inorganic Compounds and Organic Salts: Raman Spectra. Academic Press, San Diego (1997)
26. Selvaraj, U., Rao, K.J.: J. Non-Cryst. Solids **72**, 315 (1985)
27. Corbidge, D.C., Lowe, E.J.: J. Chem. Soc. Part I, 493 (1954)
28. Miller, F.A., Wilkins, C.H.: Anal. Chem. **24**, 1253 (1952)
29. Hayri, E.A., Greenblatt, M.: J. Non-Cryst. Solids **94**([3]), 387–401 (1987)
30. Williamson, G.K., Hall, W.H.: Acta Metall. **1**, 22 (1953)
31. Chowdari, B.V.R., Subba Rao, G.V., Lee, G.Y.H.: Solid State Ionics, 1067–1137 (2000)
32. Zhang, Q., Wen, Z., Liu, Y., Song, S., Wu, X.: J. Alloy Comp. **479**, 494 (2009)
33. Venkateswara Rao, G., Shashikala, H.D.: J. Alloys Compd. **622**, 108–114 (2015)
34. Duhan, S., Sanghi, S., Agarwal, A., Sheoran, A., Rani, S.: Physica B **404**, 1648 (2009)